



Article

Coupling Random Forest, Allometric Scaling, and Cellular Automata to Predict the Evolution of LULC under Various Shared Socioeconomic Pathways

Jiangfu Liao ¹, Lina Tang ^{2,*}  and Guofan Shao ³¹ Computer Engineering College, Jimei University, Xiamen 361021, China² Key Lab of Urban Environment and Health, Institute of Urban Environment, Chinese Academy of Sciences, Xiamen 361021, China³ Department of Forestry and Natural Resources, Purdue University, West Lafayette, IN 47907, USA

* Correspondence: lntang@iue.ac.cn

Abstract: Accurately estimating land-use demand is essential for urban models to predict the evolution of urban spatial morphology. Due to the uncertainties inherent in socioeconomic development, the accurate forecasting of urban land-use demand remains a daunting challenge. The present study proposes a modeling framework to determine the scaling relationship between the population and urban area and simulates the spatiotemporal dynamics of land use and land cover (LULC). An allometric scaling (AS) law and a Markov (MK) chain are used to predict variations in LULC. Random forest (RF) and cellular automata (CA) serve to calibrate the transition rules of change in LULC and realize its micro-spatial allocation (MKCA_{RF-AS}). Furthermore, this research uses several shared socioeconomic pathways (SSPs) as scenario storylines. The MKCA_{RF-AS} model is used to predict changes in LULC under various SSP scenarios in Jinjiang City, China, from 2020 to 2065. The results show that the figure of merit (FoM) and the urban FoM of the MKCA_{RF-AS} model improve by 3.72% and 4.06%, respectively, compared with the MKCA_{ANN} model during the 2005–2010 simulation period. For a 6.28% discrepancy between the predicted urban land-use demand and the actual urban land-use demand over the period 2005–2010, the urban FoM degrades by 21.42%. The growth of the permanent urban population and urban area in Jinjiang City follows an allometric scaling law with an exponent of 0.933 for the period 2005–2020, and the relative residual and R^2 are 0.0076 and 0.9994, respectively. From 2020 to 2065, the urban land demand estimated by the Markov model is 19.4% greater than the urban area predicted under scenario SSP5. At the township scale, the different SSP scenarios produce significantly different spatial distributions of urban expansion rates. By coupling random forest and allometric scaling, the MKCA_{RF-AS} model substantially improves the simulation of urban land use.

Keywords: cellular automata; urban growth; shared socioeconomic pathways; allometric scaling; land-use change



Citation: Liao, J.; Tang, L.; Shao, G. Coupling Random Forest, Allometric Scaling, and Cellular Automata to Predict the Evolution of LULC under Various Shared Socioeconomic Pathways. *Remote Sens.* **2023**, *15*, 2142. <https://doi.org/10.3390/rs15082142>

Academic Editor: Georgios Mallinis

Received: 4 March 2023

Revised: 10 April 2023

Accepted: 16 April 2023

Published: 18 April 2023



Copyright: © 2023 by the authors. Licensee MDPI, Basel, Switzerland. This article is an open access article distributed under the terms and conditions of the Creative Commons Attribution (CC BY) license (<https://creativecommons.org/licenses/by/4.0/>).

1. Introduction

In the context of global climate change, change in land use and land cover (LULC) has become one of the areas where natural and human processes most intimately intersect. On a global scale, change in LULC is affected by slow long-term effects caused by natural factors. On a regional scale, change in LULC is driven by human activities related to land use and management [1,2]. Advances in technology and medicine have led to a rapidly growing population that has created a huge demand for natural resources. This demand, which is mainly driven by human activity, appears in the form of ever-increasing changes in land use, especially urban built-up land [3]. At the same time, the high degree of homogeneity and heterogeneity of the LULC landscape dominated by human activity produces an irreversible negative impact on regional ecosystem services, such as the water

cycle, biodiversity, and climate regulation [4]. Once a highly urbanized area forms, its spatial form and development pattern are difficult to change for a long time [5]. Therefore, the double effect of change in LULC due to population growth and the negative impact of this process on the population has attracted significant research attention to the study of how changes in LULC can contribute to global environmental sustainable development [6].

Process modeling and scenario simulations of changes in LULC can reproduce the historical development dynamics of urbanized regions and can therefore be used to investigate their future spatial development patterns [7]. The emergence of GIS-based spatial data triggered the emergence of numerous techniques to simulate and analyze changes in LULC. Examples of these techniques include the intelligent cloud learning model, cellular automata (CAs), agent-based modeling, machine learning, and hybrid methods [4,8,9]. Cellular state transition and neighborhood interactions between CAs are ideally suited for expressing the process by which LULC changes, so CAs are often used to simulate and analyze changes in LULC. A CA is a lattice dynamics model with discrete time, space, and state, in which a complex system output is generated from simple interactions at the level of individual cells [10]. The characteristics of a CA model are similar to those of the complex urban system in terms of self-organization, self-replication, and the storage and transmission of information, so numerous studies have used such models to simulate urban growth [11,12].

The mining of conversion rules and the associated parametric calibration are key components of CA models used to simulate changes in LULC. Compared with traditional statistical learning techniques, machine learning algorithms and deep learning networks are better for mining the transition rules of urban CA models [13,14]. These intelligent technologies include particle swarm optimization, artificial neural networks, the random forest (RF) algorithm, fully convolutional neural networks, U-Net, and long short-term memory networks [15,16]. The deep learning network that extends the neural network is essentially a black box and is limited by computational cost, exploding and disappearing gradients, and overfitting. In contrast, the random forest algorithm better balances the performance and clearly explains the driving force contribution [17].

Numerous CA models such as CLUE-S, IDRISI, FLUS, LUSD, and PLUS divide the cell-based model of land-use change into two modules, one involving macro-scale land-use demand and one involving micro-scale changes in land use [18–22]. Multiple models or techniques were integrated into the constrained cellular-based land-use model and now serve as the basis for discerning land demand [23–25]. When overall land use is static in a particular area, growth in one type of land use must be accompanied by a decrease in another type (or types) of land use. Land-use and land cover dynamics can be interpreted as the conversion of several types of land use into a single type of land use or vice versa, thus presenting a zero-sum game of changing land-use types. For example, in areas dominated by farmland and wetlands, urban development implies the change in land use from farmland or wetland to built-up land. LULC at specific locations can change from one state to another or maintain its current state. Its state space, state sequence, change interval, and transition probability are consistent with a Markov (MK) discrete-event stochastic process.

Based on mathematical theories and observed data, a Markov chain can be used to predict the probability of changes in LULC, starting from the initial state while avoiding the data-independence assumption required by statistical methods [26,27]. Therefore, numerous studies have coupled Markov models with CAs to predict land conversion demand and simulate changes in LULC [28]. Were the analysis period restricted to several years or decades, the dynamics of land use would have their own inertia and correlation between different land-use types [29], which means that a Markov transition probability matrix based on a historical empirical analysis should accurately predict the dynamics of land-use conversion over a relatively short period [30]. However, few studies have investigated the possible biases of Markov models when predicting land demand over longer periods. Given the uncertainties faced by social and economic development, the use

of Markov models in long-term land-demand prediction over multiple cycles has yet to be evaluated [31].

Among all the socioeconomic factors that lead to changes in LULC, scaling relationships connecting urban populations and urban areas have received the most research attention [32]. The urban population is one of the most critical determinants of city size and is molded by complex regional policy factors [33]. For example, China's birth control policies and household registration system significantly affected the birth rate and regional migration of the population, which ultimately affected the population size of a region [34,35]. A clear and strong correlation exists between urban population size and urban area, although determining the exact functional form of this relationship requires further study [36]. Similar to the law of relative growth observed in the development of organisms in nature, allometric phenomena involving various components of urban systems have been evinced by numerous studies [37]. For example, Abdurashheed et al. [38] investigated the quantitative scaling relationship between clear-sky upwelling energy and the population size in 35 cities in the United Kingdom (UK). The "economy of scale" implied by the allometry slope reflects the relationship between urban form and urban size and inspires planning responses. Based on a survey of 500 cities in China, Lei et al. [39] reported that a robust scaling law exists in eight types of urban land use and population size, including residential and industrial land.

The definition of urban scale or urban boundary affects whether an allometric scaling (AS) law exists between urban population size and city size [40]. One vital factor for judging this type of human-land relationship based on geographic geometry is the shape of urban settlements. Longley, Batty, and Shepherd [36] established a theoretical urban growth model similar to the diffusion-limited aggregation (DLA) model, which is widely applied in the theoretical physics of particle clusters. This model was used to analyze empirically the urban settlement system in Norfolk, UK. The results reveal a clear allometric relationship between population size and urban settlement area, which supports the allometric scaling hypothesis proposed by Woldenberg [41] and Dutton [42]. Describing urban growth in terms of the DLA model provides a perspective for understanding why urban forms have evolved in such a "clear and unambiguous" way. This analogy suggests that the seemingly irregular evolution of urban morphology is ruled by laws similar to those that produce the DLA model or the theoretical model proposed by Longley, Batty, and Shepherd [36], as verified by empirical calculations [36,41]. The allometric relationship between population size and settlement area is an important component of these laws, so using the urban allometric scaling law to determine how urban land development reacts to changes in urban population size and to calibrate the Markov transition probability is a feasible way to model long-term patterns in LULC.

Storylines have been widely used to predict the likely dynamics of future urban growth and have proven to be an effective way to impose specific scenarios based on historical trends. Shared socioeconomic pathways (SSPs) are the core of the ScenarioMIP in the Sixth International Coupling Model Intercomparison Project. Compared with the self-defined-scenario storyline, the SSP scenario fully considers the socioeconomic factors that affect the future population size and the evolution of the urban spatial form [43]. SSP scenarios are a series of socioeconomic scenarios and emission scenarios proposed by the Intergovernmental Panel on Climate Change in 2010 to consider the challenges of mitigating and adapting to climate change. SSPs cover five scenarios: sustainable path (SSP1), middle-of-the-road path (SSP2), regional rivalry path (SSP3), inequality path (SSP4), and fossil-fuel development path (SSP5). Because it assists climate change research and facilitates comparisons between different studies, a multi-scenario analysis based on SSPs has been widely used in various fields [44]. However, few studies have explored the evolution of the urban spatial form under different SSP scenarios from the perspective of allometric scaling laws of urban systems. Constructing a new framework for deriving and predicting the future spatial development pattern of urbanized regions through the storyline of SSP population scenarios thus has potential value.

The goal of this study is to explore the allometric relationship between population size and urban area and to investigate via SSP scenarios the long-term urban land-use dynamics spanning multiple simulation periods. First, by integrating CAs into the Markov model, we construct a spatiotemporal evolution model of urban change in LULC involving various land-use types. Second, the random forest optimization algorithm is used to mine the contribution of the natural, social, and economic driving factors of land-use change and intelligently extract the occurrence probability of land-use conversion. Subsequently, the allometric scaling hypothesis is integrated into the SSP scenario framework to predict the demand for urban construction land under the different SSP population projections. Finally, the demand for urban land is used to calibrate the Markov transition probability matrix and the proposed MKCA_{RF-AS} model is applied to predict, under different SSP scenarios, the evolution of urban spatial morphology in Jinjiang City, China. The contribution of this work is thus to tightly couple the observed scaling invariance of urban systems into a highly self-calibrating urban CA model via land-use transition probabilities. This novel modeling framework is a good way to simulate the changing dynamics of urban LULC when facing large uncertainties in socioeconomic factors.

2. Study Area and Data Sources

2.1. Study Area

Jinjiang is an industrial city on the southeast coast of Fujian Province at 24°30'44"–24°54'21"N latitude and 118°24'56"–118°41'10"E longitude (Figure 1). With a land surface area of 649 km², it faces the sea on three sides: the Quanzhou bay to the northeast, the Taiwan Strait to the southeast, and Kinmen Island to the south. The city has a subtropical marine monsoon climate, with a warm and hot climate and an average annual precipitation of 1147 mm. The terrain in Jinjiang is relatively flat, and the landform types consist mainly of terraces, plains, and hills (terraces account for 67.3% of the city area). Jinjiang is a county-level city with 6 subdistricts and 13 towns under its jurisdiction. As of 1 November 2020, the city's resident population was 2.062 million, and its population density of 3177 people/km² ranked second among districts and counties in China [45]. Figure 1 shows the geographical location, topographic features, land use, and population density of Jinjiang City in 2020. Areas A, B, and C are located in the northeast, midwest, and south of Jinjiang City, respectively. The land use of area A is dominated by urban land, and its average population density exceeds 3877 people/km². Land use in areas B and C mainly involves urban land and agricultural land. Areas B and C have lower population densities than area A. Jinjiang City is an industrial city dominated by advanced manufacturing and has many industrial clusters with a scale of over 100 billion or 10 billion CNY, such as shoes and clothing, textiles, building materials, equipment, and medical care. Its gross domestic product in 2021 is 298.64 billion CNY, and it is the district and county that ranks first in the output value of the secondary industry in Fujian Province [46]. The rapid industrialization of the past few decades has led to the continuous and rapid expansion of urban land, so a large amount of cultivated land has been converted into construction land. According to the 14th Five-Year Plan, the per capita gross domestic product of Jinjiang City in 2035 is expected to be twice that of 2020, and the rapid expansion of urban land in the coming period will still be the main feature of regional changes in land use. However, in the mid-to-long term (i.e., beyond 2050), China's overall population will slowly decline [47]. This makes the highly industrialized area of Jinjiang City an excellent region to explore how the medium- and long-term land-use dynamics will evolve under SSP scenarios.

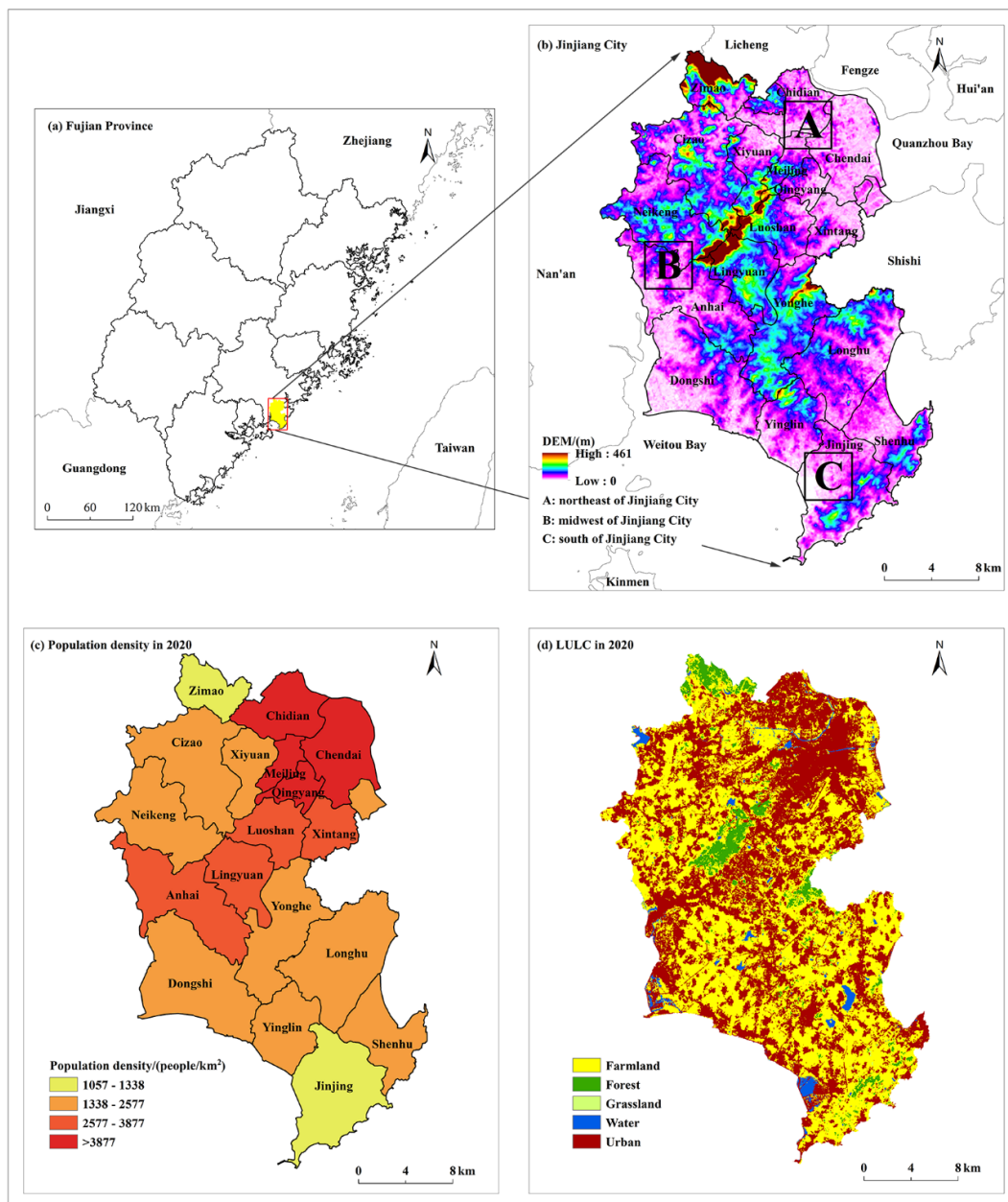


Figure 1. Case study area: Jinjiang, Fujian Province, China.

2.2. Data Source

The basic data used in this study include LULC data, traffic and cadastral data, socioeconomic data, urban development planning data, and population data for SSP scenarios. LULC data (2005–2020) were obtained by interpreting and processing Landsat TM/ETM+ remote sensing images based on the Google Earth Engine (GEE) platform. This dataset combines data from Landsat TM and ETM+ sensors before 2013, and only uses Landsat 8 Operational Land Imager (OLI) data after 2013 (available at <http://code.earthengine.google.com>, last accessed 6 August 2021). Yang and Huang [48] interpreted the data. This set of LULC year-by-year datasets covers 5 types of land use, including agricultural land, forest land, grassland, built-up land, and water, and has a spatial resolution of $30\text{ m} \times 30\text{ m}$. Traffic and cadastral data mainly include the location of administrative centers at various levels: expressways, railways, main roads, and township administrative division maps. Because Jinjiang City is located in the Quanzhou Plain and occupies a flat terrain, the elevation and slope are excluded from the factors driving the change in LULC. The selected driving

factors include distance to the city center, distance to the town center, distance to a train station, distance to the airport, distance to a highway, distance to the railway, distance to the main road, and distance to the coastline. The population socioeconomic data come from the statistical yearbook of Jinjiang City from 2005 to 2020 and mainly involve data from permanent urban residents. Population data include the sixth and seventh national household census data from 2010 and 2020. The standard time points of the two censuses are 0:00 on 1 November 2010 and 2020, respectively. The permanent resident population in the census includes the following three situations: (1) population residing in the given township with household registration in the township, (2) population living in the township and leaving the registered township for more than half a year, and (3) population with household registration in the township and less than half a year away from the township. The urban development planning data come from the 14th Five-Year Plan outline of Jinjiang national economic and social development (2020–2035). The SSP scenario data come from the gridded datasets for China’s urban and rural population from 2020 to 2100 under SSP1–5, which was released by Jiang et al. from Nanjing University of Information Science and Technology and with a resolution of $0.5^\circ \times 0.5^\circ$. The dataset was downscaled to 1 km resolution through Kriging interpolation to obtain the urban population size of Jinjiang City from 2020 to 2100.

3. Methods

3.1. Calibrating Transition Rules Using Random Forest

Random forest is a dual-state classifier composed of multiple decision trees, and its output state is determined by the mode of the state vectors output by all subtrees [49]. Random forest adopts a random selection strategy with replacement from the original dataset when constructing the dataset for the sub-decision tree and uses the undrawn samples as the test set to evaluate its prediction error. At the same time, random forest subtrees randomly select feature subsets for each split node from all features and on this basis determine the optimal classification feature for the given node [50]. These random strategies endow the sub-decision trees with sufficient diversity, thereby ensuring the optimal performance of the random forest classification algorithm. When using random forest to mine the transition rules of the urban CA model, the original dataset consists of cells in the cellular grid, and the features consist of elements in the driving force vector. In this study, the random forest module in the PLUS model is used to mine the contribution of different factors driving change in LULC [17]. In the urban land-use evolution model, the formula for obtaining the probability of land-use conversion using the random forest classification algorithm is

$$P_{ij,k}^r = \frac{\sum_{n=1}^M I(h_n(v) = r)}{M}, \quad (1)$$

where $P_{ij,k}^r$ is the probability that the state of cell (i, j) transforms into land-use type k , v is the vector of the factors driving change in LULC, $h_n(v)$ is the prediction type of the n th decision tree after inputting the independent variable $v(v_1, v_2, \dots, v_i, \dots, v_n)$, and r is a binary value (0 or 1), where 1 means that other land-use types change to type k , and 0 means otherwise. M is the number of sub-decision trees and $I(\cdot)$ is the indicative function of the decision tree set and returns 1 (0) when the $h_n(v) = r$ (otherwise). In the urban CA model, the driving factor v_i is the independent variable or feature in the random forest classifier. Therefore, a significant advantage of mining cellular transition rules with random forests is the ability to assess the importance of each factor in the driving-factor vector to the dependent variable [17]. By adding random noise to the corresponding out of bag at the sub-decision tree feature v_i , calculating the change in out-of-bag error helps to accurately estimate the importance of feature v_i [51].

3.2. Coupling an Allometric Scaling Law and the Markov Chain to Predict Demand for Change in LULC

A Markov chain describes a random motion process in a discrete index set and state space. The conditional probability of its state transition has no aftereffect [52]. Under a specific spatiotemporal background, change in LULC in urbanized areas shows a mutual transformation relationship, and the average transfer state of land-use structure remains relatively stable. Therefore, for the spatiotemporal evolution of urban land-use systems with multiple land-use types, the Markov model is appropriate for predicting the demand for change in LULC [28]. The key to using a Markov chain to predict the demand for urban land-use conversion is to construct the transition probability matrix [27]

$$P = (P_{ij}) = \begin{pmatrix} P_{11} & P_{12} & \dots & P_{1M} \\ P_{21} & P_{22} & \dots & P_{2M} \\ \dots & \dots & P_{ii} & \dots \\ P_{M1} & P_{M2} & \dots & P_{MM} \end{pmatrix}, \quad (2)$$

where P_{ij} is the probability that the i th land-use type converts to the j th land-use type between time T and $T + 1$. The value of P_{ij} is obtained from the occurrence frequency of the transition from land-use type i to land-use type j during the period (i.e., the conversion area counted in units of cells divided by the total area of land-use type i at time T). M is the number of land-use types, and each element P_{ij} of the transition probability matrix satisfies the conditions [53]

$$\begin{cases} 0 \leq P_{ij} \leq 1, & i, j = 1, 2, \dots, M \\ \sum_{j=1}^M P_{ij} = 1, & i = 1, 2, \dots, M. \end{cases} \quad (3)$$

Most studies calculate the area of converted land-use types by using the historical land-use data from two points in time and then calculate the transition probability matrix for this period.

The transition probability matrix of the Markov model objectively reflects the status of land-use conversion between different land-use types and is suitable for predicting the evolution of land use and the corresponding demand for land use. However, the Markov transition probability matrix is usually calculated based on historical land-use data, and less consideration is given to socioeconomic or other driving factors. However, socioeconomic models or land-use planning on the regional macro-scale should be used to obtain the development demand for urban land and to revise the transition probability matrix output by the Markov model.

The evolution of urban spatial patterns generally follows the allometric scaling law [54], which condemns each part of the urban system to a different speed of development (i.e., the relative growth rate of one element of urban development such as population size and that of another element such as urban area are proportional) [55]. The longitudinal allometric growth model is generally used to analyze the expansion of urban land use. Longitudinal allometries describe the evolution of a dynamic process over time by using time series or corresponding sample paths based on observational data. The mathematical expression of the longitudinal allometric growth model is generally based on a power-law relationship [32],

$$A_t = \alpha(P_t)^b, \quad (4)$$

where t is the period of the historical land-use data or statistical information, A_t is the urban area at time t , P_t is the urban population size at time t , α is a proportionality coefficient, and b is a constant scaling exponent, generally representing the ratio of the relative growth rate of urban built-up land to that of population size. Thus, if the parameters α and b are determined from historical data, the area of urban built-up land can be estimated based on demographic predictions of population size.

If A_a and A_m are, respectively, used to represent the area of new urban construction land predicted by the allometric model and the Markov model, and the ratio of A_a to A_m is denoted ψ_j , the Markov transition probability matrix can be revised as follows: (1) Multiplying ψ_j by the probability of converting other land-use types into urban land, the probability of non-conversion of urban land remains unchanged. (2) By using ψ_i multiplied by the probability that land use i is converted into a non-urban land use ($i \neq j$), the revised Markov transition probability matrix using the allometric growth model takes the form

$$P' = (P'_{ij}) = \begin{pmatrix} \psi_1 P_{11} & \psi_1 P_{12} & \dots & \psi_j P_{1j} & \dots & \psi_1 P_{1M} \\ \psi_2 P_{21} & \psi_2 P_{22} & \dots & \psi_j P_{2j} & \dots & \psi_2 P_{2M} \\ \dots & \dots & \dots & \dots & \dots & \dots \\ \psi_i P_{i1} & \psi_i P_{i2} & \dots & \psi_j P_{ij} & \dots & \psi_i P_{iM} \\ \dots & \dots & \dots & \dots & \dots & \dots \\ P_{j1} & P_{j2} & \dots & P_{jj} & \dots & P_{jM} \\ \dots & \dots & \dots & \dots & \dots & \dots \\ \psi_M P_{M1} & \psi_M P_{M2} & \dots & \psi_j P_{Mj} & \dots & \psi_M P_{MM} \end{pmatrix}, \tag{5}$$

where ψ_i and ψ_j are the correction coefficients of the above transition probability matrix, and subscript j means urban land. The correction factor ψ_i is calculated by the following formula:

$$\psi_i = \frac{1 - \psi_j P_{ij}}{\sum_{l=1}^M P_{il} - P_{ij}}, \quad i = 1, 2, \dots, M; i \neq j, \tag{6}$$

where l is the land-use subscript in the transition probability matrix, i is the subscript of land-use types other than urban land, j is the subscript of urban land use, and P_{il} is the probability that land use i will be transformed into land use l .

3.3. Using Cellular Automata to Allocate Micro-Spatial Changes in LULC

The suitability of various land uses obtained by the random forest algorithm and the demand for land-use conversion output by the Markov model were input into the MKCA_{RF-AS} model to simulate the evolution of LULC. In this study, the Markov model and CA model were designed and implemented by using Matlab (MathWorks, Natick, MA, USA). To simulate the micro-spatial allocation based on CAs, the transition rules are critical to obtaining suitable land use at each location. The transition rules generally use cell state, neighborhood state, and land conversion potential to estimate the probability of land-use changes in cells. The state of a cell at time t is a function of the cell state at $t - 1$, the neighborhood state at time $t - 1$, and many other factors. Its general form is as follows [56]:

$$S_{ij}^t = f(S_{ij}^{t-1}, P_{c,ij}, \Omega_{ij}^{t-1}, Cons, R) \tag{7}$$

where S_{ij}^t and S_{ij}^{t-1} are the states of cell (i, j) at times t and $t - 1$, respectively; $P_{c,ij}$ is the cell's land conversion potential (i.e., the developmental suitability of cell (i, j)); Ω_{ij}^{t-1} is the distribution of specific LULC in the neighboring space of cell (i, j) ; $Cons$ is a constraint mechanism that restricts land-use conversion; R is a random factor that simulates the uncertainty of land-use dynamics; and f is a series of transition rules that determines changes in cell state.

The neighborhood interaction is one of the core components of a cellular-based land-use evolution model. The number of cells of various LULCs in the neighborhood changes as the cellular model evolves. The state of a cell is directly affected by the distribution of land-use types in the neighborhood. The most abundant land-use types in the neighborhood often determine the future transition state of the central cell. The neighborhood function based on a square neighborhood window can be constructed as follows [57]:

$$\Omega_{ij,k}^{t-1} = \frac{\sum_q^{m \times m} con(S_{ij}^{t-1} = k)(q \neq 1)}{m \times m - 1}, \tag{8}$$

where $\Omega_{ij,k}^{t-1}$ is the value of the neighborhood function that affects the conversion of the central cell (i, j) to land use k , and $con(S_{ij}^{t-1} = k)$ is the number of cells of land use k in the $m \times m$ moving window neighborhood with cell (i, j) as the center.

If a local probability expresses development suitability, then the probability is generally affected by a series of spatial distance variables. The values of each spatial variable at sample points are extracted as independent variables and input into the random forest model to obtain the local probability that the cell be converted to a specific land use. After adding factors such as random perturbation and constraints to the cellular model, the final total conversion probability of the central cell is [58]

$$P_{total,k}^t = [1 + (-\ln \gamma)^\alpha] P_{c,ij} \Omega_{ij,k}^{t-1} \times Cons(S_{ij,k}^{t-1}), \quad (9)$$

where t is the iterative sequence of cellular automaton evolution, $P_{total,k}^t$ is the probability of conversion to land use k at time t , $1 + (-\ln \gamma)^\alpha$ is a random disturbance term reflecting the uncertainty of an urban system [59], γ is a random number between 0 and 1, α is an integer between 1 and 10, $\Omega_{ij,k}^{t-1}$ is the neighborhood influence, and $Cons(\cdot)$ is a constraining function constrains the change in cell states.

3.4. Scenario Setting

China has implemented a universal two-child population policy since 2015 [60]. We use the scenario settings based on this policy and the global SSPs framework to carry out urban population estimates for China's 5 SSP scenarios from 2020 to 2100 [47]. Based on the allometric relationship between population and area in the urban system, this research predicts various future scenarios of urban land demand as a function of different population scenario storylines. The evaluation considers the basic factors affecting population development, such as fertility rate, mortality rate, migration rate, and education level in historical periods. It also calibrates parameters and verifies the population-development-environment model.

The SSP scenario depicts the current status of social and economic development and the following possible future development trends: (1) In the SSP1 scenario, regional development gradually shifts toward a relatively sustainable green development path, which emphasizes human well-being while reducing inequalities within countries. (2) The SSP2 scenario is an intermediate path between SSP1 and SSP3. Under this scenario, the region's population, economy, and urbanization will not deviate significantly from the historical development path. (3) In the SSP3 scenario, the revival of nationalism prompts countries to focus on domestic or regional problems. The region experiences slow economic development and urbanization, and the decline in education and investment worsens social inequality. (4) In the SSP4 scenario, income inequality within and between countries increases and becomes significantly stratified. Human capital investment and economic development opportunities are highly unequal, resulting in high levels of development in high-tech industries but low income and educational opportunities in labor-intensive sectors. (5) The SSP5 scenario adopts a resource- and energy-intensive lifestyle, and each country's technology, economy, and population develop rapidly.

3.5. Method for Evaluating Accuracy

In this work, the overall accuracy (OA), Kappa coefficient, and figure of merit (FoM) are used to qualify the simulation of the proposed model. The overall accuracy and Kappa coefficient provide a comparative analysis at the pixel level. The calculation superimposes the real and simulated maps and constructs a confusion matrix based on a point-to-point comparison. The FoM quantifies the consistency of land-use transition patterns and is obtained by overlaying and analyzing the initial, actual, and simulated maps. The FoM is the fraction of correctly predicted land use to the overall land use in the simulation results [61]:

$$FoM = \frac{B}{A + B + C + D'} \quad (10)$$

where B is the number of cells where the land use changes and the simulated scenario also produces the correct transition; A is the number of cells whose land use actually changes, whereas the simulated land use remains unchanged; C is the number of cells in which both the observed data and the simulated results change, but the resulting land uses differ; and D is the number of cells where the actual land use does not change, but the simulated land use changes.

4. Simulation Results

4.1. Land-Use Suitability

The 2005–2010 land-use data and driving factors were input into the land-use expansion analysis strategy (LEAS) module of the PLUS model to intelligently mine the land development suitability of the MKCA_{RF-AS} model [17]. The LEAS module is driven by the random forest algorithm. The sampling method in its parameter configuration is random sampling; there are 20 decision trees, the sampling rate is 0.05, and 8 features participate in the training. The results output by the LEAS module of the PLUS model reflect the suitability for the development of land use on a scale of 1 to 255. In Jinjiang City, the change in land use from 2005 to 2010 mainly involves the expansion of urban land. Figure 2 shows the suitability of urban land development extracted by the random forest algorithm and the importance of the driving factors. In general, the main urban area in the northeast, the satellite towns in the south, and the central region and the west are all highly suitable for development from 2005 to 2010. The top 3 drivers contributing to urban development are the distance to main roads, distance to railway stations, and distance to railways, and the relative importance is 0.2164, 0.1270, and 0.1238, respectively. As a typical industrial city, the urbanization of Jinjiang depends strongly on the transportation infrastructure.

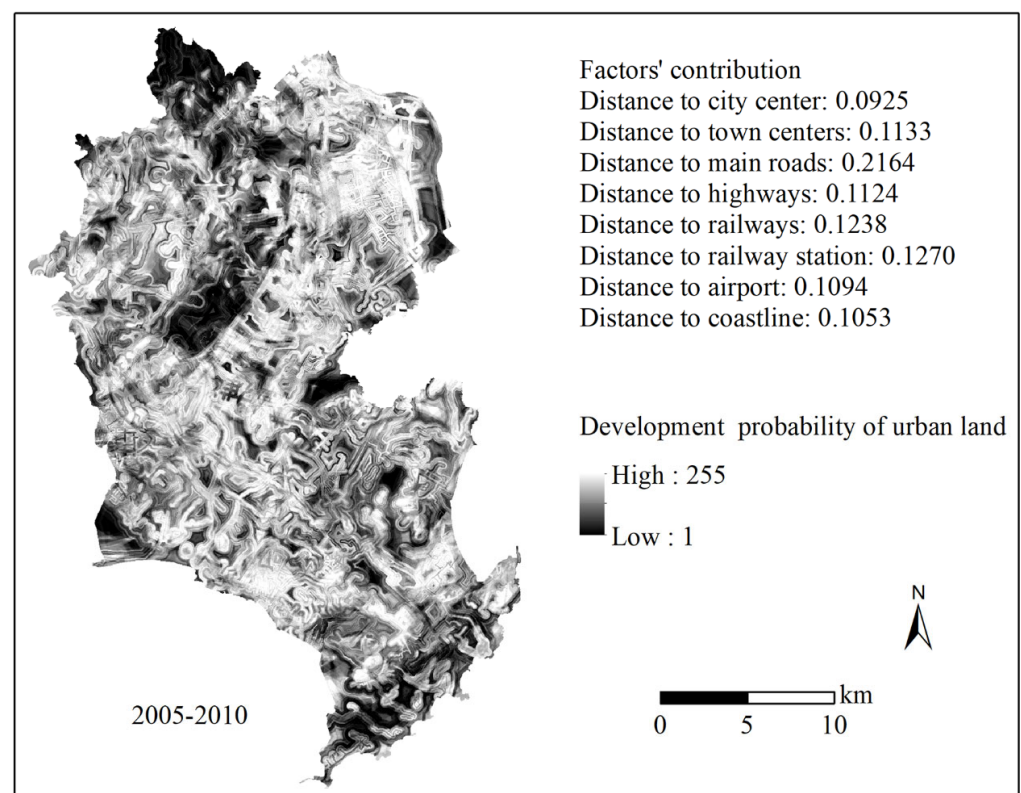


Figure 2. Suitability of urban land development mined by random forest algorithm in Jinjiang City from 2005 to 2010.

4.2. Simulation of Spatial Distribution of LULC

We input the obtained suitability of land-use development into the $MKCA_{RF-AS}$ model and simulated the spatial distribution of land during 2005–2010 (see Figure 3). Analyzing and comparing the spatial details, Figure 3a,b,e show that forest land, grassland, and water body are the smallest three land-use types. Woodland and grassland are mainly distributed in the northern and central parts, and water bodies are mainly distributed in lakes, rivers, and depressions around Quanzhou Bay and Weitou Bay. Cultivated land and construction land are the two most widely distributed land-use types in the study area. The construction land is mainly distributed in the coastal plain area with flat terrain and well-developed transportation, and its expansion mainly comes from the occupation of cultivated land. The expansion of construction land mainly occurs in the central urban area in the northeast, the satellite cities in the central and western regions, and the industrial technology innovation corridor between them. The land-use spatial pattern simulated in Figure 3e is similar to that in Figure 3b. Based on the point-to-point overlay analysis, the evaluation metrics of the FoM, urban FoM, overall accuracy, and Kappa coefficient are 25.5%, 35.0%, 84.2%, and 0.709, respectively. Studies show that the FoM is more accurate than the Kappa coefficient for evaluating the simulation of land-use change models, and the FoM and urban FoM of the $MKCA_{RF-AS}$ model both have high values in the literature [62].

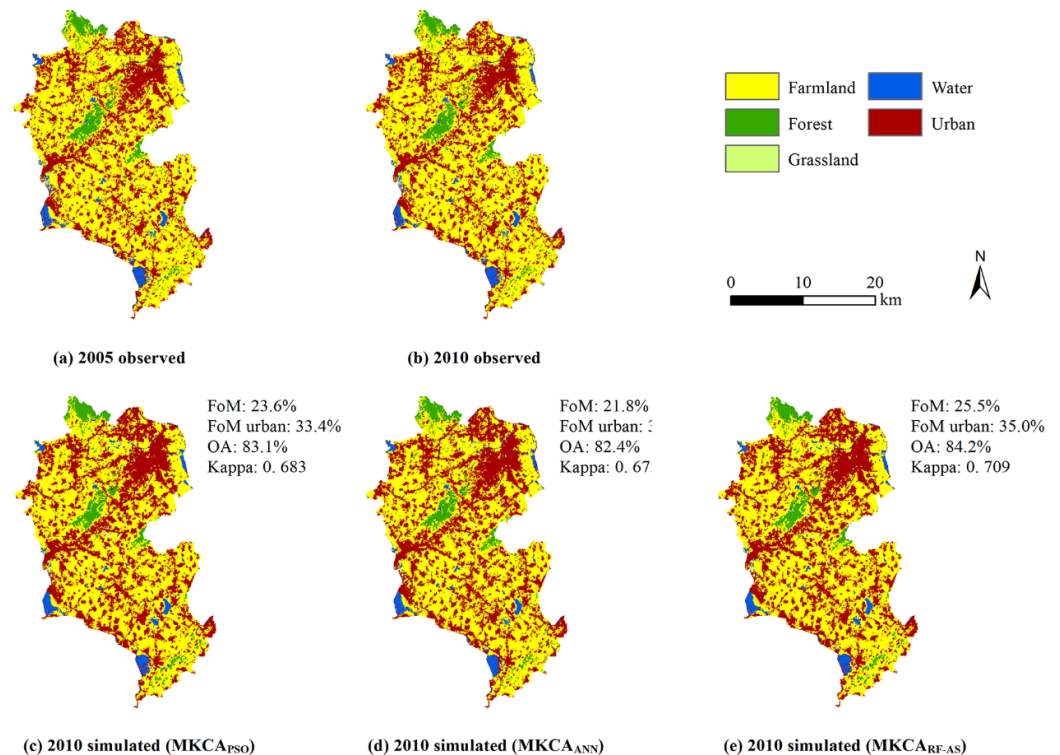


Figure 3. Comparison of spatial distribution of LULC simulated using different cellular automata models.

Particle swarm optimization (PSO) and the artificial neural network (ANN) are typical artificial intelligence algorithms and perform well in the automatic calibration of the transition rules of urban CA models [63,64]. To verify the ability of the random forest algorithm to mine the transition rules of urban LULC change models, this work selects PSO and ANN as references for comparative research. To test the simulation of $MKCA_{RF-AS}$, $MKCA_{PSO}$ and $MKCA_{ANN}$ were used to simulate the spatiotemporal evolution of the LULC over the same period. The results show that the above four accuracy indicators are significantly greater for the $MKCA_{RF-AS}$ model than for the $MKCA_{PSO}$ or $MKCA_{ANN}$ models. For example, the FoM and urban FoM produced by the $MKCA_{RF-AS}$ model are 3.72% and 4.06% greater than

that produced by the MKCA_{ANN} model. The MKCA_{RF-AS} model is thus an effective tool for simulating land-use change and explaining the driving factors.

4.3. Sensitivity Analysis

To explore how different configurations of land-use demand affect the simulation results of the MKCA_{RF-AS} model, we carried out a sensitivity analysis of the model based on the land-use demand predicted by the Markov model spanning multiple periods. The simulation covers the three periods of 2005–2010, 2005–2015, and 2005–2020, and the land-use conversion demand is calculated by using the Markov transition probability matrix extracted from the period 2000–2005. Considering the difference between the actual urban land-use demand in the above 3 periods and the values predicted by the Markov model, 2% was selected as the minimum change for the sensitivity analysis (see Table 1). Compared with the FoM, the urban FoM is more sensitive to changes in urban land-use demand. During the period 2005–2010, when the urban land-use demand changed from 261,381 cells (actual value in 2010) to 244,954 cells (predicted value of Markov model), the urban FoM decreased from 35.02% to 27.52%. In other words, an error of 6.28% in the predicted urban land-use demand changes the urban FoM by 21.42%. When the predicted demand for urban land use in the two periods 2005–2015 and 2005–2020 produces similar errors, the urban FoM decreases by 17.43% and 17.57%, respectively. At the same time, when the error in urban land-use demand reaches 2%, the decrease in the urban FoM differs for different simulation periods. This sensitivity analysis illustrates that the error of predicted land-use demand amplifies the spatial error in the simulation of the change in LULC.

Table 1. Sensitivity of the MKCA_{RF-AS} model to demand for urban land use.

Changes in Demand for Urban Land Use	2005–2010			2005–2015			2005–2020		
	Urban Land (Cells)	FoM (%)	Urban FoM (%)	Urban Land (Cells)	FoM (%)	Urban FoM (%)	Urban Land (Cells)	FoM (%)	Urban FoM (%)
Predicted change in land use by Markov model	244,954	23.45	27.52	263,221	27.21	32.40	277,949	21.37	27.76
+2%	249,853	24.31	29.95	268,485	27.46	33.74	283,508	21.48	28.55
+2%	254,752	24.78	32.05	273,750	27.75	35.11	289,067	21.57	29.31
+2%				279,014	28.00	36.43	294,626	21.76	30.18
+2%				284,279	28.19	37.63	300,185	21.96	31.13
+2%							305,744	21.97	31.85
+2%							311,303	22.21	32.79
Actual demand for urban land use	261,381	25.48	35.02	292,024	28.27	39.24	318,210	22.21	33.68

4.4. Allometric Relations between Population Size and Urban Area

The least squares method was used to fit the allometric growth equation to the permanent urban population as a function of the urbanized land area during the period 2005–2020, and the results are shown in Table 2. The urban area uses the classification data of the urban land use from the LULC yearly dataset obtained from remote sensing images from 2005 to 2020, and the permanent urban population comes from the statistical yearbook and national census data. The results show that the coefficient of proportionality $\alpha = 2.800$, the scale index $b = 0.933$, the relative residual is 0.0076, and the $R^2 = 0.9994$. The 2005–2020 urban area predicted by the calibrated allometric model is very close to the observed result. The urban area predicted by the calibrated allometric model closely matches the observed data for the period 2005–2020.

Table 2. Allometric scaling analysis of population size and urban area in Jinjiang from 2005 to 2020.

Year	2005	2006	2007	2008	2009	2010	2011	2012	2013	2014	2015	2016	2017	2018	2019	2020
POP	67.7	72.2	74.0	76.7	80.9	117.3	120.7	124.9	128.4	132.2	133.5	135.8	139.0	141.4	142.8	141.6
POP-SSNPC	94.8	101.1	103.5	107.4	113.3	117.3	118.5	122.7	126.1	129.8	131.1	133.4	136.5	138.9	140.3	141.6
UBA	200.4	207.7	213.7	218.7	228.4	235.6	241.4	246.8	253.4	259.6	263.2	267.9	274.9	281.2	285.6	286.4
UBA-AS	195.7	207.7	212.4	219.8	231.1	238.6	241.0	249.0	255.4	262.4	264.9	269.0	275.0	279.5	282.0	284.6

Note: POP: resident population (urban) (10^4), POP-SSNPC: revised population data from the Sixth and Seventh National Population Censuses (10^4), UBA: urban area (km^2), UBA-AS: urban area predicted by the allometric scaling model (km^2).

This research revises the statistical data for 2005–2020 based on the results of the Sixth and Seventh National Population Censuses conducted in 2010 and 2020. The data from the Sixth National Population Census (2010) differ significantly from that in 2009. For example, the permanent urban population in 2009 and 2010 was 809,200 and 1,172,800, respectively, an increase of 44.9%. Considering that the average annual growth rate of the urban resident population in 2005–2009 was between 2.49% and 6.65%, the statistics for 2005–2009 are revised upward by 40%. Similarly, according to the Seventh National Population Census data (2020), the statistical data for 2011–2019 are revised downward by 1.78%. The population data for 2005–2020 were revised by two national household censuses and are highly accurate. This greatly enhances the reliability of the analysis of the allometric relationship between urban population size and urban area.

4.5. Predicting Urban Land-Use Demand for 2020–2100

Figure 4a shows the storyline of Jinjiang’s population growth from 2020 to 2100 under the various SSP scenarios after the localization calibration. The calibration first sets the population size in 2020 under the SSP scenarios to the actual population in 2020, and the correction coefficient obtained is then used to proportionally adjust the population data in future years under each SSP scenario. Figure 4b uses the 2005–2020 Markov transition probability matrix to predict the urban area of Jinjiang City in 2035, 2050, 2065, 2080, 2095, and 2110. Furthermore, we linearly interpolate to obtain year-by-year population forecasts for 2020–2100. At the same time, the parameters obtained for the allometric growth model are used to predict the urban area from 2020 to 2100 under the various SSP scenarios. The results show that the urban area predicted by the Markov model in 2020–2100 even exceeds that of the SSP5 scenario. When using a Markov model to predict long-term urban land-use demand, the results may deviate significantly from the baseline or even in the opposite direction.

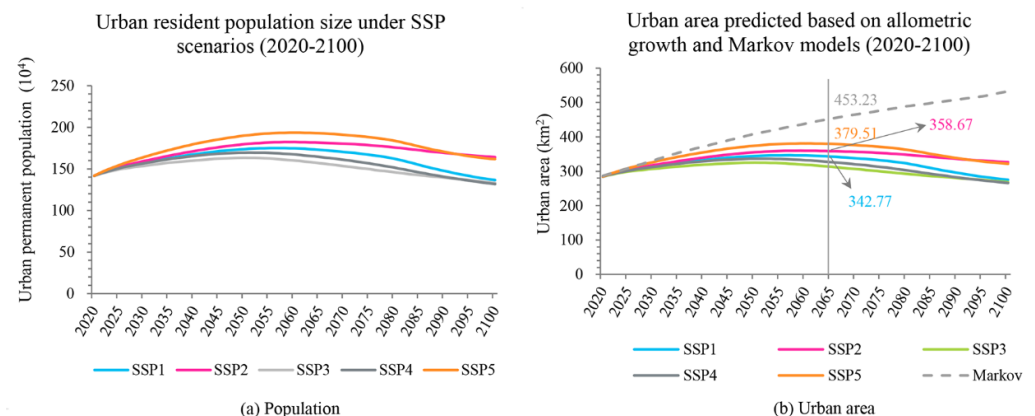


Figure 4. Predicted population size and urban area in Jinjiang City from 2020 to 2100 under the different SSP scenarios.

4.6. Spatiotemporal Evolution of LULC from 2020 to 2065

4.6.1. Correction of Transition Probability Matrix

To measure the demand for land-use conversion from 2020 to 2065, the Markov transition probability matrix from 2005 to 2020 is revised based on the urban area obtained

under each SSP scenario in 2065. Table 3 summarizes the transition probability under typical SSP scenarios of the initial land-use type to the target land-use type (including no change in land-use type). The results show that, under each SSP scenario and compared with 2005–2020, the probability of transforming agricultural land, grassland, and water bodies into built-up land decreases significantly, while forest land and built-up land do not change significantly. For example, under the SSP5 scenario, the probabilities of transforming agricultural land, grassland, and water into built-up land decreases from 0.1948, 0.6031, and 0.2561 during 2005–2020 to 0.0994, 0.2826, and 0.1260, respectively. Figure 4b shows the projection of urban area for the period 2020–2100 in the Markov model, calculated based on the transition probability matrix from 2005 to 2020. Therefore, the comparison confirms the negative impact of the slower growth trend of urban land use on the Markov transition probability under the SSP scenarios. Conversely, the probability that cultivated land remains unchanged increases significantly under each SSP scenario. This probability increases from the original values of 0.7829 to 0.9132, 0.8966, and 0.8740 under the scenarios SSP1, SSP2, and SSP5, respectively. The probability of forest land, grassland, and water bodies remaining unchanged also increases to a certain extent.

Table 3. Corrected Markov transition probability matrices for three SSPs scenarios during 2020–2065.

SSP Scenarios	Probability of Shifting to the Following Land-Use Type				
	Agricultural	Woodland	Grassland	Water	Built-Up
2005–2020					
Agricultural	0.7829	0.0166	0.0018	0.0039	0.1948
Woodland	0.3092	0.6653	0.0005	0.0001	0.0249
Grassland	0.3487	0.0068	0.0327	0.0088	0.6031
Water	0.2218	0.0004	0.0024	0.5193	0.2561
Built-up	0.0004	0.0000	0.0000	0.0025	0.9971
2020–2065 (SSP1)					
Agricultural	0.9132	0.0211	0.0021	0.0051	0.0585
Woodland	0.2895	0.6989	0.0004	0.0000	0.0114
Grassland	0.7454	0.0161	0.0476	0.0306	0.1606
Water	0.2870	0.0002	0.0030	0.6366	0.0733
Built-up	0.0002	0.0000	0.0000	0.0022	0.9976
2020–2065 (SSP2)					
Agricultural	0.8966	0.0206	0.0021	0.0050	0.0757
Woodland	0.2913	0.6943	0.0004	0.0000	0.0142
Grassland	0.7043	0.0150	0.0409	0.0287	0.2114
Water	0.2793	0.0003	0.0029	0.6223	0.0953
Built-up	0.0002	0.0000	0.0000	0.0022	0.9975
2020–2065 (SSP5)					
Agricultural	0.8740	0.0198	0.0021	0.0048	0.0994
Woodland	0.2941	0.6881	0.0004	0.0000	0.0175
Grassland	0.6402	0.0133	0.0385	0.0257	0.2826
Water	0.2685	0.0003	0.0027	0.6025	0.1260
Built-up	0.0003	0.0000	0.0000	0.0023	0.9975

4.6.2. Scenario Simulation

We used the revised Markov transition probability matrix and the area of various land-use types in 2020 to predict the area where the land-use type changes from 2020 to 2065. The resulting land-use demand was then input into the MKCA_{RF-AS} model to simulate the 2065 spatial distribution of land use in Jinjiang City under various SSP scenarios (Figure 5). The simulation results show that agricultural land and built-up land are the most important land-use types in the study area. Although the development trend is slow, the main change in the LULC under each SSP scenario during 2020–2065 remains the continuous sprawl of urban land. Over time, the development of urban built-up land is particularly significant in the northeastern, central, western, and southern regions. By 2065, due to the continuous expansion of the main urban area and the implementation of the strategy of integrating Quanzhou Bay, a large-scale high-density urban area should appear to the northeast of Jinjiang City (see Figure 5, enlarged area A). At the same time, affected by the radiation of Xiamen City, the west and south should develop satellite-city clusters that would play an important role in supporting the aggregation and development of the

central urban area. Conversely, the comparison of enlarged areas B and C in Figure 5 under different SSP scenarios shows that construction land expansion under SSP2 and SSP5 is significantly faster than under the other SSP scenarios. Driven by the dense transportation network and the integration of urban and rural areas, Jinjiang should develop a medium-to-high-density urbanization area within the city under the scenarios SSP2 and SSP5.

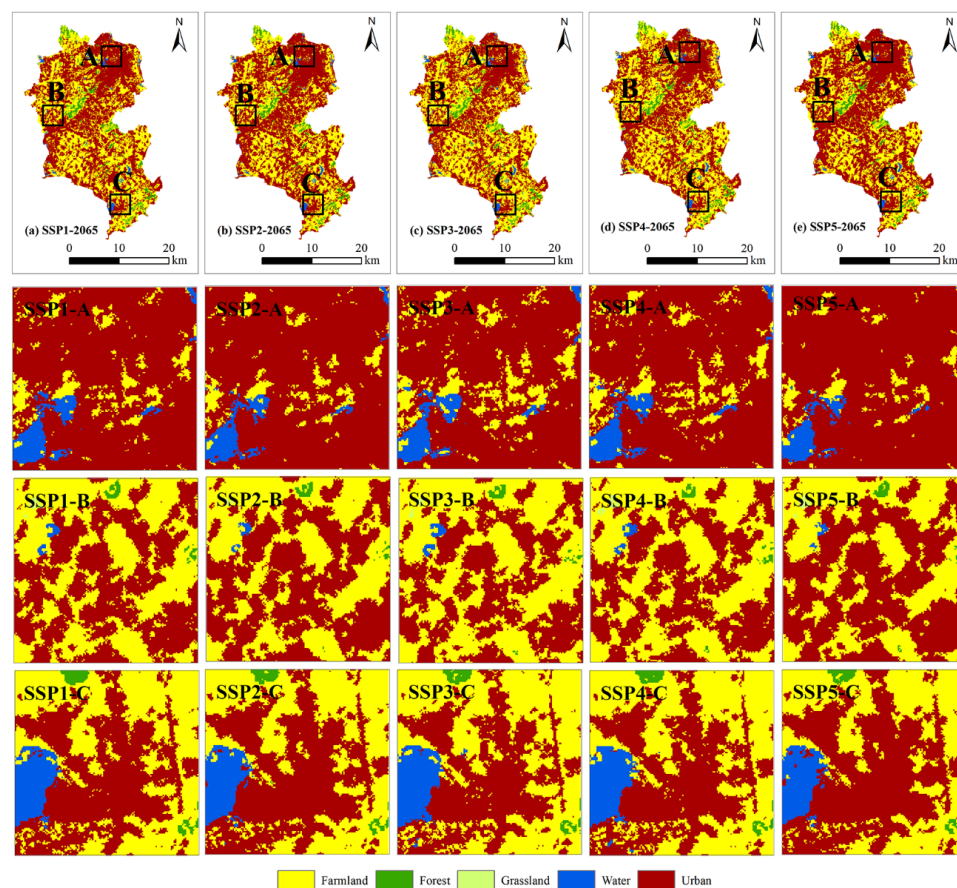


Figure 5. Simulation of LULC changes in Jinjiang City from 2020 to 2065 under five SSP scenarios.

Table 4 lists the percent change in the land-use area under the different SSP scenarios over 2020–2065. The percent change in the LULC in 2065 depends strongly on the SSP scenario. For example, the percent change in the urban land (agricultural land) area under SSP5 is 3.49 (3.73) times that under SSP3. In all SSP scenarios, the expansion of built-up land is counter-balanced by a reduction in the area of other land-use types. Agricultural land changes relatively little under some SSP scenarios, such as -6.7% and -10.7% under scenarios SSP3 and SSP4. However, the reduction in agricultural land area is larger under each SSP scenario than that of forest land, grassland, and water bodies. In particular, under scenarios SSP1, SSP2, and SSP5, the area of agricultural land reduction is 49.88, 64.63, and 83.58 km², respectively.

Table 4. Areas assigned to different land uses and the percent change in land-use area over the period 2020–2065 under the different SSP scenarios.

Land-Use Types	2020	2065	2020–2065	2065	2020–2065	2065	2020–2065	2065	2020–2065	2065	2020–2065
	Area (km ²)	(SSP1) Area (km ²)	(SSP1) %	(SSP2) Area (km ²)	(SSP2) %	(SSP3) Area (km ²)	(SSP3) %	(SSP4) Area (km ²)	(SSP4) %	(SSP5) Area (km ²)	(SSP5) %
Agricultural	331.36	281.47	−15.05	266.72	−19.51	308.92	−6.77	296.15	−10.62	247.78	−25.22
Woodland	25.44	23.23	−8.67	22.39	−11.99	24.83	−2.40	24.03	−5.54	21.51	−15.44
Grassland	0.92	0.70	−23.90	0.68	−26.63	0.80	−12.78	0.74	−19.71	0.65	−29.56
Water	11.84	8.36	−29.37	8.18	−30.87	9.10	−23.12	8.70	−26.49	7.84	−33.80
Built-up	286.39	342.63	19.64	358.43	25.16	312.94	9.27	326.89	14.14	378.92	32.31

4.6.3. Analysis of Urban Expansion on the Township Scale

Figure 6 depicts the spatial distribution of the urbanization rate on the township scale based on the calculated growth rate of the urban area over the period 2020–2065. Under scenario SSP1, which continues the historical development trend, most regions show a medium rate of development. Under scenario SSP4 (unbalanced development pathway), the entire region develops at a medium-low rate. The spatial distribution of the urban development rate of scenarios SSP2, SSP3, and SSP5 differs significantly. Under scenario SSP2, the urbanization rate of most towns in the west, central, and eastern regions is medium, whereas under scenarios SSP3 and SSP5, most of these towns develop at a low or high rate. The development rate of streets or townships in the northeast and central urban areas is relatively low, which is closely related to the high urbanization rate in this area at the beginning of the simulation. The analysis of the township-scale urbanization rate under scenarios such as SSP2 and SSP5 provides an objective reference for the urban hierarchy in the spatial planning of land use.

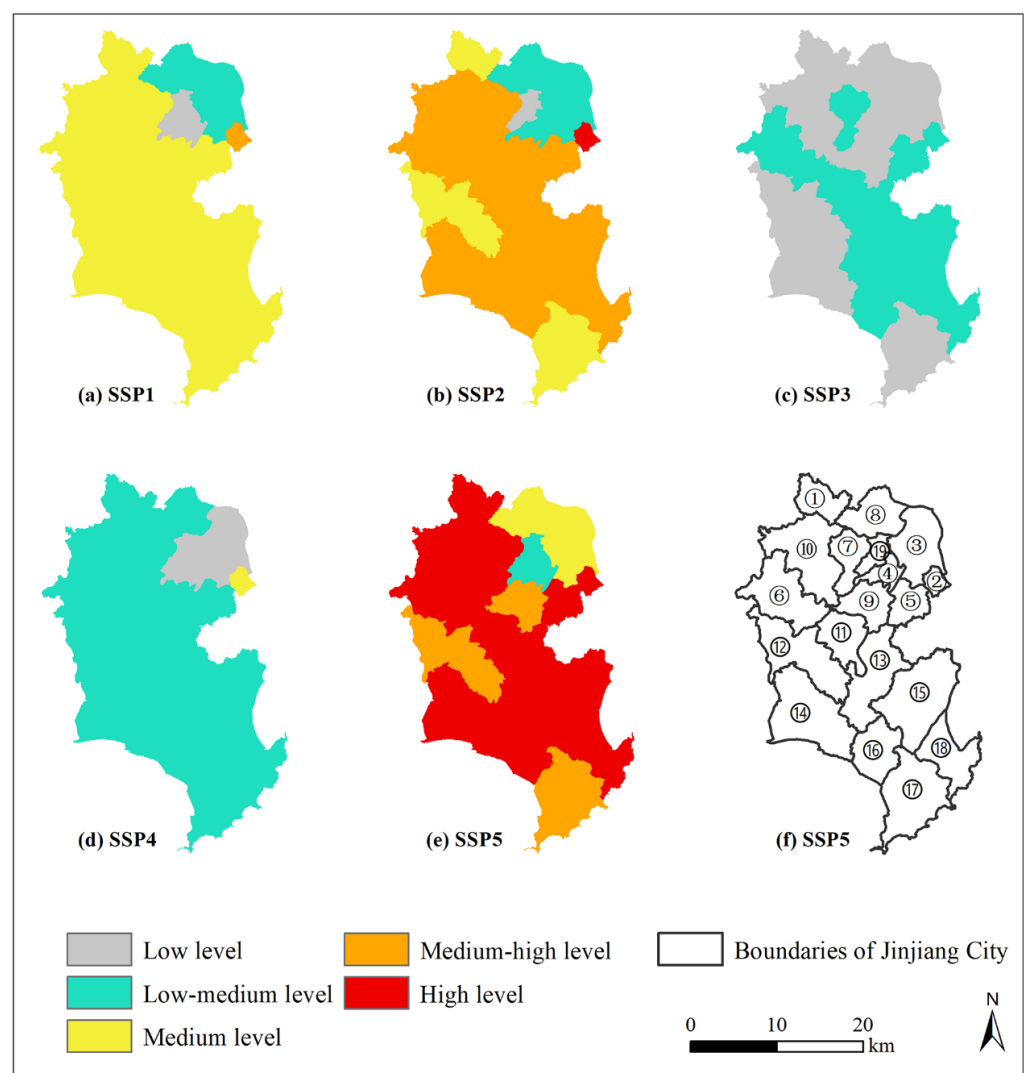


Figure 6. Spatial distribution of rate of expansion of Jinjiang City under the different SSP scenarios from 2020 to 2065. The town numbers in panel (f) are assigned as follows: ① Zimao, ② Xibin, ③ Chendai, ④ Qingyang, ⑤ Xintang, ⑥ Neikeng, ⑦ Xiyuan, ⑧ Chidian, ⑨ Luoshan, ⑩ Cizao, ⑪ Lingyuan, ⑫ Anhai, ⑬ Yonghe, ⑭ Dongshi, ⑮ Longhu, ⑯ Yinglin, ⑰ Jinjing, ⑱ Shenhu, and ⑲ Meiling.

5. Discussion

The scaling exponent of the allometric growth model has a clear geographical meaning. The two most important characteristics of cities are the concentration of population and the more intense use of urban material resources [54]. This study investigates the scale invariance associated with complex urban development. In other words, we are interested in the range and ideal value of the scaling exponent in the scale invariance of an urban system. Bettencourt [54] analyzed the urban infrastructure and socioeconomic metrics of metropolitan areas in the United States in 2006 and calculated the scaling exponents governing the scaling relationship between (i) the gross domestic product and population and (ii) the roads and population to be 0.849 and 1.126, respectively. At the same time, Bettencourt [54] claims that the superlinear scaling exponent for wealth, innovation, and crime in urban systems is about 1.15 (7/6), and the sublinear scaling exponent for infrastructure networks such as roads and cables is about 0.85 (5/6). Bettencourt [54] concludes that sublinear scaling means the material infrastructure saved per capita as cities grow. Moreover, the scaling exponent of the urban infrastructure network with respect to population size is more sublinear than that of the urban area. Nordbeck [65] considered that, because people are active in three-dimensional space and urban expansion occurs on a two-dimensional plane, the allometric exponent should be $2/3$. Recently, Bettencourt [54] proposed a microscopic urban growth model that considers the hierarchical organization of infrastructure networks, which theoretically confirms the $2/3$ scaling exponent between population size and urban area.

Lee [66] concluded that the allometric exponent of urban growth should fluctuate between $2/3$ and 1. If the dimensions of population and urban area are assumed to be 2 and 1.7, respectively, then the theoretical value of the scaling exponent should be close to 0.85 [67]. Based on an empirical analysis of typical cities around the world, Lee [66] concluded that the scaling exponents between population size and urban area in the United States, Japan, and Canada in 1960 were 0.8757, 0.9140, and 0.874, respectively. Cao et al. [32] used the population density flow diagram to describe the 6 development levels of China's urban agglomerations, and the scaling exponents between the population size and urban area fall in the range [0.79, 0.95]. Based on the data input during 2005–2020, the scaling exponent of the allometric relationship between population size and urban area in Jinjiang is 0.933. Strictly speaking, when the scaling exponent is greater than 1, the expansion rate of urban construction land is greater than the growth rate of the urban population. When the scaling exponent is equal to 1, the relative rate of urban land area expansion equals the relative growth of the urban population. When the scaling exponent is less than 1, the relative rate of expansion of urban land is less than the relative growth of the urban population. With the expansion of urban land area, the land area in the urban system of Jinjiang City is efficiently used, on average. If compared with the theoretical value of the scaling exponent, the urban land use of Jinjiang City can be planned and designed in a more compact form. This means that Jinjiang can explore an intensive development path with a greater economic value per unit land area [68].

Natural biological organisms have undergone long-term adaptation and evolution, so allometric scaling phenomena (weight/volume) are widely observed [69]. The spatial expansion of urban areas is often driven or constrained by natural conditions, historical culture, and socioeconomic factors. Scaling relations thus appear in the context of individual cities and urban agglomerations between population size and urban area or between other components of urban systems [32,70]. The large differences in factors that influence urban regions and their selection or adaptation produce different scaling relations. The existing literature divides the values of scaling exponents into positive or negative allometry based on a threshold of 1 or 0.85 [71,72]. In contrast with this method of categorization, we assign positive allometric growth to the case of urban expansion and negative allometric growth to urban contraction. This categorization scheme makes it vital to simulate urban shrinkage from the perspective of the negative allometric growth of population size and urban area.

Conversely, a new research focus involves combining remote sensing measurement technology and CA to deduce the three-dimensional growth process of urbanized areas [73]. Based on accurate measurements of the area and volume of built-up urbanized areas, the scaling relationship between population size and urban volume and its scaling exponents can be further clarified. In this way, population size can be used to predict the building volumes of an urban area. Considering urban volume as a macro demand and combining CA and allometric scaling to simulate the horizontal and vertical growth of three-dimensional urban space is also a new field to be explored.

This research revises the Markov transition probability matrix for long time series to span multiple periods. We use the Markov transition probability matrix from 2000 to 2005 to predict the demand for land use from 2005 to 2020, which helps to test the advantages and limitations of the Markov chain for estimating land-use demand across multiple cycles. The results in Table 1 show that the error ratio between the predicted urban land use and the observed urban land use in 2020 reaches 12.7% when using the transition probability matrix from 2000 to 2005 to predict the land-use demand from 2005 to 2020. However, predicting land-use demand from 2020 to 2065 based on the transition probability matrix from 2005 to 2020 covers 3 15-year Markov forecast periods. Figure 4 shows the predicted urban land-use demand in 2065 under the 3 scenarios SSP1, SSP2, and SSP5. The results differ from Markov's predicted value by 32.2%, 26.4%, and 19.4% respectively. The Markov model underestimates the observed value in the previous prediction and overestimates predictions based on the SSPs scenarios for 2065. This result indicates that Markov chains may be more suitable for predicting land-use demand over relatively short periods that involve fewer cycles. When the driving factors remain unchanged or the uncertainties faced in the future are relatively small, appropriately extending the forecast time or expanding the number of forecast periods can produce credible results.

This work focuses on the scaling relationship between the population size and urban area in urban systems and the future evolution of urban LULC. In this context, changes in population size are the critical factors influencing urban land demand and the spatiotemporal evolution of LULC in urban systems. Population size is affected by factors such as fertility, mortality, migration, and education level. With the continuous advancement of industrialization and urbanization, the employment pressure and living cost of urbanites are increasing. Meanwhile, newborn survival rates and people's education level continue to improve. These compounding factors make the process of urbanization lead to a significant decline in people's willingness to have children in most countries around the world [74].

The SSP scenario sets the story line of the future population and economic development based on population and human resources, economic development, lifestyle, human development, environment and natural resources, policy and system, and technological development. SSP scenarios fully describe the opportunities, potentials, and uncertainties facing the future population and economic development. Therefore, considering the development uncertainty of socioeconomic factors, the urban areas predicted by the SSP scenario and the Markov model differ significantly (Figure 4b). The implication of this finding to the environmental remote sensing science literature is that the integration of allometric scaling laws for population size and urban area is a candidate for more effective urban simulations if the uncertainties due to population size are considered.

The spatial pattern of the urban expansion rate predicted in Figure 6 provides an important reference for analyzing the consequences of urbanization, such as the heat-island effect, water shortage, and loss of cultivated land. First, under all SSP scenarios, we must focus on the urban heat-island problem in densely populated areas, such as the northeast and around Quanzhou Bay. At the same time, under the SSP5 scenario, the development path driven by fossil energy will expand industrial, residential, and commercial urban land at a super-high rate during 2020–2065. The heat-island effect of major satellite cities also must be considered. Second, the population density of Jinjiang City in 2022 was as high as 3177 people/km², and its spatiotemporal distribution is relatively uneven at the township scale (Figure 1c). With the continuous advancement of the urbanization process

under different SSP scenarios, the population density will continue to increase and show significant spatial differentiation. Jinjiang City is a city with scarce water resources. In 2020, its per capita water resources and per capita comprehensive water consumption were $62 \text{ m}^3/\text{person}$ and $276 \text{ m}^3/\text{person}$, respectively [75]. The possible water resource stress in densely populated areas under different SSP scenarios and its coping strategies should be further studied. Finally, the expansion of urban land in Jinjiang City is mainly at the expense of occupying cultivated land, which means that the city's food demand will rely more on the production of other regions. At the same time, the food demand of the region will drive the development of arable land away from Jinjiang City to other regions. We must further study this teleconnection effect of LULC changes under different SSP scenarios from the county scale [76].

The Intergovernmental Panel on Climate Change estimates that the possible rise in the global mean sea level by 2100 will range between 0.29 m and 1.10 m [77]. Jinjiang City is surrounded by the sea on three sides, the elevation of most areas in the coastal zone is 1–4 m, and the elevation of some low-lying areas is less than 1 m. In addition, Jinjiang City is densely populated in the urban center and in satellite cities around Quanzhou Bay and Weitou Bay, and large quantities of cultivated land are distributed in coastal depressions. It is thus urgent to analyze the exposure risk and loss of population and economic output that may result from the average rise in sea level and the 100-year-storm surge under different SSP scenarios.

6. Conclusions

This research proposes the $\text{MKCA}_{\text{RF-AS}}$ urban model, which combines an allometric scaling law, a Markov chain, the random forest algorithm, and cellular automata to simulate future scenarios of land use under various shared social development pathways. The FoM and urban FoM obtained by the $\text{MKCA}_{\text{RF-AS}}$ model for urban growth simulations from 2005 to 2010 are 25.5% and 35.0%, respectively, and the urban FoM is 4.06% greater than that produced by the MKCA_{ANN} model. To verify the scaling relations between the population size and urban area, this research revises the Markov transition probability matrix and predicts the spatiotemporal evolution of LULC for 2020–2065. The results lead to the following conclusions:

(1) Prediction errors may occur when using the Markov model to predict long-term land-use demand spanning multiple periods. The error between the predicted urban land-use demand based on the transition probability matrix for the period 2000–2005 and the observed urban land-use demand in 2020 is 12.7%. (2) The scaling exponent relating the population growth and urban area of Jinjiang City from 2005 to 2020 is 0.933. The relative rate of urban land area expansion is less than the relative growth rate of the population, which reflects an efficient use of land in the urban system of Jinjiang. (3) The simulation accuracy of the $\text{MKCA}_{\text{RF-AS}}$ model depends strongly on land-use demand. While the Markov model produces an error of 6.28% when predicting urban land use during 2005–2010, the FoM declines by 21.42%. (4) Most townships in Jinjiang City develop at medium and high rates under scenarios SSP2 and SSP5. Based on the assumption of allometric scaling between the population size and urban area, the prediction of LULC provides an objective reference for spatial land-use planning.

Given the prevalence of allometric scaling phenomena in urban systems, this work focuses on integrating allometric scaling between the population size and urban area into the proposed model. In the future, we will explore and verify how scaling invariance affects the evolution of urban spatial forms in a larger urban area and over a longer time span.

Author Contributions: Conceptualization, J.L. and L.T.; methodology, J.L. and L.T.; software, J.L.; validation, J.L.; formal analysis, L.T.; investigation, J.L.; resources, L.T. and G.S.; data curation, L.T.; writing—original draft preparation, J.L.; writing—review and editing, L.T. and G.S.; visualization, J.L.; supervision, L.T. and G.S.; project administration, L.T.; funding acquisition, L.T. All authors have read and agreed to the published version of the manuscript.

Funding: This study was supported by the National Natural Science Foundation of China (NSFC) (Grant No. 41471137).

Data Availability Statement: Not applicable.

Conflicts of Interest: The authors declare no conflict of interest.

References

1. Beillouin, D.; Cardinael, R.; Berre, D.; Boyer, A.; Corbeels, M.; Fallot, A.; Feder, F.; Demenois, J. A global overview of studies about land management, land-use change, and climate change effects on soil organic carbon. *Glob. Chang. Biol.* **2022**, *28*, 1690–1702. [[CrossRef](#)] [[PubMed](#)]
2. Ahammad, R.; Hossain, M.K.; Sobhan, I.; Hasan, R.; Biswas, S.R.; Mukul, S.A. Social-ecological and institutional factors affecting forest and landscape restoration in the Chittagong Hill Tracts of Bangladesh. *Land Use Policy* **2023**, *125*, 106478. [[CrossRef](#)]
3. De Olivera, L.C.M.; de Mendonça, G.C.; Costa, R.C.A.; de Camargo, R.A.L.; Fernandes, L.F.S.; Pacheco, F.A.L.; Pissarra, T.C.T. Impacts of urban sprawl in the Administrative Region of Ribeirão Preto (Brazil) and measures to restore improved landscapes. *Land Use Policy* **2023**, *124*, 106439. [[CrossRef](#)]
4. Sun, Y.; Liu, D.; Wang, P. Urban simulation incorporating coordination relationships of multiple ecosystem services. *Sustain. Cities Soc.* **2022**, *76*, 103432. [[CrossRef](#)]
5. Domingo, D.; Van Vliet, J.; Hersperger, A.M. Long-term changes in 3D urban form in four Spanish cities. *Landscape Urban Plan.* **2023**, *230*, 104624. [[CrossRef](#)]
6. Jia, B.; Luo, X.; Wang, L.; Lai, X. Changes in Water Use Efficiency Caused by Climate Change, CO₂ Fertilization, and Land Use Changes on the Tibetan Plateau. *Adv. Atmos. Sci.* **2023**, *40*, 144–154. [[CrossRef](#)]
7. Black, B.; van Strien, M.J.; Adde, A.; Grêt-Regamey, A. Re-considering the status quo: Improving calibration of land use change models through validation of transition potential predictions. *Environ. Model. Softw.* **2023**, *159*, 105574. [[CrossRef](#)]
8. Chen, Y.; Weng, Q.; Tang, L.; Wang, L.; Xing, H.; Liu, Q. Developing an intelligent cloud attention network to support global urban green spaces mapping. *ISPRS J. Photogramm. Remote Sens.* **2023**, *198*, 197–209. [[CrossRef](#)]
9. Sun, S.; Parker, D.C.; Brown, D.G. From an agent-based laboratory to the real world: Effects of “neighborhood” size on urban sprawl. *Comput. Environ. Urban Syst.* **2023**, *99*, 101889. [[CrossRef](#)]
10. Feng, Y.; Gao, C.; Wang, R.; Li, P.; Xi, M.; Jin, Y.; Tong, X. A moving window-based spatial assessment method for dynamic urban growth simulations. *Geocarto Int.* **2022**, *37*, 15282–15301. [[CrossRef](#)]
11. Zhang, B.; Hu, S.; Wang, H.; Zeng, H. A size-adaptive strategy to characterize spatially heterogeneous neighborhood effects in cellular automata simulation of urban growth. *Landscape Urban Plan.* **2023**, *229*, 104604. [[CrossRef](#)]
12. Molinero-Parejo, R.; Aguilera-Benavente, F.; Gómez-Delgado, M.; Shurupov, N. Combining a land parcel cellular automata (LP-CA) model with participatory approaches in the simulation of disruptive future scenarios of urban land use change. *Comput. Environ. Urban Syst.* **2023**, *99*, 101895. [[CrossRef](#)]
13. Halder, S.; Das, S.; Basu, S. Use of support vector machine and cellular automata methods to evaluate impact of irrigation project on LULC. *Environ. Monit. Assess.* **2023**, *195*, 3. [[CrossRef](#)] [[PubMed](#)]
14. Shojaei, H.; Nadi, S.; Shafizadeh-Moghadam, H.; Tayyebi, A.; Van Genderen, J. An efficient built-up land expansion model using a modified U-Net. *Int. J. Digit. Earth* **2022**, *15*, 148–163. [[CrossRef](#)]
15. Liu, J.; Xiao, B.; Li, Y.; Wang, X.; Bie, Q.; Jiao, J. Simulation of dynamic urban expansion under ecological constraints using a long short term memory network model and cellular automata. *Remote Sens.* **2021**, *13*, 1499. [[CrossRef](#)]
16. Wu, X.; Liu, X.; Zhang, D.; Zhang, J.; He, J.; Xu, X. Simulating mixed land-use change under multi-label concept by integrating a convolutional neural network and cellular automata: A case study of Huizhou, China. *GIScience Remote Sens.* **2022**, *59*, 609–632. [[CrossRef](#)]
17. Liang, X.; Guan, Q.; Clarke, K.C.; Liu, S.; Wang, B.; Yao, Y. Understanding the drivers of sustainable land expansion using a patch-generating land use simulation (PLUS) model: A case study in Wuhan, China. *Comput. Environ. Urban Syst.* **2021**, *85*, 101569. [[CrossRef](#)]
18. Luo, Z.; Zhang, W.; Wang, Y.; Wang, T.; Liu, G.; Huang, W. Spatial optimization of ecological ditches for non-point source pollutants under urban growth scenarios. *Environ. Monit. Assess.* **2023**, *195*, 105. [[CrossRef](#)]
19. Chasia, S.; Olang, L.O.; Sitoki, L. Modelling of land-use/cover change trajectories in a transboundary catchment of the Sio-Malaba-Malakisi Region in East Africa using the CLUE-s model. *Ecol. Model.* **2023**, *476*, 110256. [[CrossRef](#)]
20. Lin, X.; Wang, Z. Landscape ecological risk assessment and its driving factors of multi-mountainous city. *Ecol. Indic.* **2023**, *146*, 109823. [[CrossRef](#)]

21. Ou, M.; Li, J.; Fan, X.; Gong, J. Compound Optimization of Territorial Spatial Structure and Layout at the City Scale from “Production–Living–Ecological” Perspectives. *Int. J. Environ. Res. Public Health* **2023**, *20*, 495. [[CrossRef](#)]
22. Ren, Q.; He, C.; Huang, Q.; Zhang, D.; Shi, P.; Lu, W. Impacts of global urban expansion on natural habitats undermine the 2050 vision for biodiversity. *Resour. Conserv. Recycl.* **2023**, *190*, 106834. [[CrossRef](#)]
23. Isinkaralar, O.; Varol, C.; Yilmaz, D. Digital mapping and predicting the urban growth: Integrating scenarios into cellular automata—Markov chain modeling. *Appl. Geomat.* **2022**, *14*, 695–705. [[CrossRef](#)]
24. Ouyang, X.; Xu, J.; Li, J.; Wei, X.; Li, Y. Land space optimization of urban-agriculture-ecological functions in the Changsha-Zhuzhou-Xiangtan Urban Agglomeration, China. *Land Use Policy* **2022**, *117*, 106112. [[CrossRef](#)]
25. Yang, J.; Tang, W.; Gong, J.; Shi, R.; Zheng, M.; Dai, Y. Simulating urban expansion using cellular automata model with spatiotemporally explicit representation of urban demand. *Landsc. Urban Plan.* **2023**, *231*, 104640. [[CrossRef](#)]
26. Overmars, K.P.; De Koning, G.H.J.; Veldkamp, A. Spatial autocorrelation in multi-scale land use models. *Ecol. Model.* **2003**, *164*, 257–270. [[CrossRef](#)]
27. Arsanjani, J.J.; Helbich, M.; Kainz, W.; Boloorani, A.D. Integration of logistic regression, Markov chain and cellular automata models to simulate urban expansion. *Int. J. Appl. Earth Obs. Geoinf.* **2013**, *21*, 265–275. [[CrossRef](#)]
28. Isinkaralar, O.; Varol, C. A cellular automata-based approach for spatio-temporal modeling of the city center as a complex system: The case of Kastamonu, Türkiye. *Cities* **2023**, *132*, 104073. [[CrossRef](#)]
29. Van Vliet, J.; Naus, N.; Van Lammeren, R.J.; Bregt, A.K.; Hurkens, J.; Van Delden, H. Measuring the neighbourhood effect to calibrate land use models. *Comput. Environ. Urban Syst.* **2013**, *41*, 55–64. [[CrossRef](#)]
30. Liao, J.; Tang, L.; Shao, G. Multi-Scenario Simulation to Predict Ecological Risk Posed by Urban Sprawl with Spontaneous Growth: A Case Study of Quanzhou. *Int. J. Environ. Res. Public Health* **2022**, *19*, 15358. [[CrossRef](#)]
31. Zhang, S.; Zhong, Q.; Cheng, D.; Xu, C.; Chang, Y.; Lin, Y.; Li, B. Landscape ecological risk projection based on the PLUS model under the localized shared socioeconomic pathways in the Fujian Delta region. *Ecol. Indic.* **2022**, *136*, 108642. [[CrossRef](#)]
32. Cao, W.; Dong, L.; Cheng, Y.; Wu, L.; Guo, Q.; Liu, Y. Constructing multi-level urban clusters based on population distributions and interactions. *Comput. Environ. Urban Syst.* **2023**, *99*, 101897. [[CrossRef](#)]
33. Aretouyap, Z.; Abdelfattah, M.; Gaber, A. Urban sprawl analysis and shoreline extraction in Douala-Cameroon city using optical and radar sensors. *Geocarto Int.* **2022**, *37*, 14596–14608. [[CrossRef](#)]
34. Wang, H.; Guo, F. City-level socioeconomic divergence, air pollution differentials and internal migration in China: Migrants vs talent migrants. *Cities* **2023**, *133*, 104116. [[CrossRef](#)]
35. Yang, L.; Guo, J.; Cao, S. What structural factors have held back China’s birth rate? *Environ. Dev. Sustain.* **2022**, 1–14. [[CrossRef](#)]
36. Longley, P.A.; Batty, M.; Shepherd, J. The size, shape and dimension of urban settlements. *Trans. Inst. Br. Geogr.* **1991**, *16*, 75. [[CrossRef](#)]
37. Kaufmann, T.; Radaelli, L.; Bettencourt, L.M.; Shmueli, E. Scaling of urban amenities: Generative statistics and implications for urban planning. *EPJ Data Sci.* **2022**, *11*, 50. [[CrossRef](#)]
38. Abdulrasheed, M.; MacKenzie, A.R.; Whyatt, J.; Chapman, L. Allometric scaling of thermal infrared emitted from UK cities and its relation to urban form. *City Environ. Interact.* **2020**, *5*, 100037. [[CrossRef](#)]
39. Lei, W.; Jiao, L.; Xu, G. Understanding the urban scaling of urban land with an internal structure view to characterize China’s urbanization. *Land Use Policy* **2022**, *112*, 105781. [[CrossRef](#)]
40. Chen, Y. Multi-scaling allometric analysis for urban and regional development. *Phys. A Stat. Mech. Appl.* **2017**, *465*, 673–689. [[CrossRef](#)]
41. Woldenberg, M.J. An allometric analysis of urban land use in the United States. *Ekistics* **1973**, *36*, 282–290.
42. Dutton, G. Criteria of growth in urban systems. *Ekistics* **1973**, *36*, 298–306.
43. Wang, X.; Meng, X.; Long, Y. Projecting 1 km-grid population distributions from 2020 to 2100 globally under shared socioeconomic pathways. *Sci. Data* **2022**, *9*, 563. [[CrossRef](#)] [[PubMed](#)]
44. Li, Z.; Murshed, M.; Yan, P. Driving force analysis and prediction of ecological footprint in urban agglomeration based on extended STIRPAT model and shared socioeconomic pathways (SSPs). *J. Clean. Prod.* **2023**, *383*, 135424. [[CrossRef](#)]
45. JCSB. Bulletin of the Seventh National Population Census of Jinjiang City. 2021. Available online: http://www.jinjiang.gov.cn/xxgk/zfxgkzl/bmzfxgk/tjj/zfxgkml/202105/t20210531_2565668.htm (accessed on 8 January 2023).
46. JCSB—Jinjiang City Statistics Bureau and National Bureau of Statistics of China. *Jinjiang Statistical Yearbook in 2022*; China Statistics Press: Beijing, China, 2022.
47. Jiang, T.; Su, B.; Wang, Y.; Wang, G.; Luo, Y.; Zhai, J.Q.; Huang, J.; Jing, C.; Gao, M.; Lin, Q. Gridded datasets for population and economy under Shared Socioeconomic Pathways for 2020–2100. *Adv. Clim. Chang. Res.* **2022**, *18*, 381–383.
48. Yang, J.; Huang, X. The 30 m annual land cover dataset and its dynamics in China from 1990 to 2019. *Earth Syst. Sci. Data* **2021**, *13*, 3907–3925. [[CrossRef](#)]
49. Breiman, L. Random forests. *Mach. Learn.* **2001**, *45*, 5–32. [[CrossRef](#)]
50. Ren, L.; Seklouli, A.S.; Zhang, H.; Wang, T.; Bouras, A. An adaptive Laplacian weight random forest imputation for imbalance and mixed-type data. *Inf. Syst.* **2023**, *111*, 102122. [[CrossRef](#)]
51. Pan, Y.; Kong, X.; Yuan, Y.; Sun, Y.; Han, X.; Yang, H.; Zhang, J.; Liu, X.; Gao, P.; Li, Y. Detecting the foreign matter defect in lithium-ion batteries based on battery pilot manufacturing line data analyses. *Energy* **2023**, *262*, 125502. [[CrossRef](#)]

52. Wu, J.; Zhao, R.; Sun, J. State transition of carbon emission efficiency in China: Empirical analysis based on three-stage SBM and Markov chain models. *Environ. Sci. Pollut. Res.* **2023**, 1–11. [[CrossRef](#)]
53. Girma, R.; Fürst, C.; Moges, A. Land use land cover change modeling by integrating artificial neural network with cellular Automata-Markov chain model in Gidabo river basin, main Ethiopian rift. *Environ. Chall.* **2022**, *6*, 100419. [[CrossRef](#)]
54. Bettencourt, L.M. The origins of scaling in cities. *Science* **2013**, *340*, 1438–1441. [[CrossRef](#)] [[PubMed](#)]
55. Chen, Y. Scaling, fractals and the spatial complexity of cities. In *Handbook on Cities and Complexity*; Edward Elgar Publishing: Cheltenham, UK, 2021.
56. Feng, Y.; Wang, R.; Tong, X.; Zhai, S. Comparison of change and static state as the dependent variable for modeling urban growth. *Geocarto Int.* **2022**, *37*, 6975–6998. [[CrossRef](#)]
57. Wang, H.; Guo, J.; Zhang, B.; Zeng, H. Simulating urban land growth by incorporating historical information into a cellular automata model. *Landsc. Urban Plan.* **2021**, *214*, 104168. [[CrossRef](#)]
58. Lin, J.; Li, X.; Wen, Y.; He, P. Modeling urban land-use changes using a landscape-driven patch-based cellular automaton (LP-CA). *Cities* **2023**, *132*, 103906. [[CrossRef](#)]
59. White, R.; Engelen, G. Cellular automata and fractal urban form: A cellular modelling approach to the evolution of urban land-use patterns. *Environ. Plan. A* **1993**, *25*, 1175–1199. [[CrossRef](#)]
60. Zeng, Y.; Hesketh, T. The effects of China's universal two-child policy. *Lancet* **2016**, *388*, 1930–1938. [[CrossRef](#)]
61. Pontius, R.G.; Boersma, W.; Castella, J.-C.; Clarke, K.; de Nijs, T.; Dietzel, C.; Duan, Z.; Fotsing, E.; Goldstein, N.; Kok, K. Comparing the input, output, and validation maps for several models of land change. *Ann. Reg. Sci.* **2008**, *42*, 11–37. [[CrossRef](#)]
62. Liu, X.; Liang, X.; Li, X.; Xu, X.; Ou, J.; Chen, Y.; Li, S.; Wang, S.; Pei, F. A future land use simulation model (FLUS) for simulating multiple land use scenarios by coupling human and natural effects. *Landsc. Urban Plan.* **2017**, *168*, 94–116. [[CrossRef](#)]
63. Xu, T.; Gao, J.; Coco, G. Simulation of urban expansion via integrating artificial neural network with Markov chain–cellular automata. *Int. J. Geogr. Inf. Sci.* **2019**, *33*, 1960–1983. [[CrossRef](#)]
64. Feng, Y.; Liu, Y.; Tong, X.; Liu, M.; Deng, S. Modeling dynamic urban growth using cellular automata and particle swarm optimization rules. *Landsc. Urban Plan.* **2011**, *102*, 188–196. [[CrossRef](#)]
65. Nordbeck, S. Urban allometric growth. *Geogr. Ann. Ser. B Hum. Geogr.* **1971**, *53*, 54–67. [[CrossRef](#)]
66. Lee, Y. An allometric analysis of the US urban system: 1960–80. *Environ. Plan. A* **1989**, *21*, 463–476. [[CrossRef](#)] [[PubMed](#)]
67. Chen, Y.; Feng, J. A hierarchical allometric scaling analysis of Chinese cities: 1991–2014. *Discret. Dyn. Nat. Soc.* **2017**, *2017*, 5243287. [[CrossRef](#)]
68. Bettencourt, L.M.; Lobo, J.; Helbing, D.; Kühnert, C.; West, G.B. Growth, innovation, scaling, and the pace of life in cities. *Proc. Natl. Acad. Sci. USA* **2007**, *104*, 7301–7306. [[CrossRef](#)]
69. Lynch, M.; Trickovic, B.; Kempes, C.P. Evolutionary scaling of maximum growth rate with organism size. *Sci. Rep.* **2022**, *12*, 22586. [[CrossRef](#)]
70. Jia, Y.; Tang, L.; Zhang, P.; Xu, M.; Luo, L.; Zhang, Q. Exploring the scaling relations between urban spatial form and infrastructure. *Int. J. Sustain. Dev. World Ecol.* **2022**, *29*, 665–675. [[CrossRef](#)]
71. Veregin, H.; Tobler, W.R. Allometric relationships in the structure of street-level databases. *Comput. Environ. Urban Syst.* **1997**, *21*, 277–290. [[CrossRef](#)]
72. Lv, M.; Chen, Z.; Yao, L.; Dang, X.; Li, P.; Cao, X. Potential Zoning of Construction Land Consolidation in the Loess Plateau Based on the Evolution of Human–Land Relationship. *Int. J. Environ. Res. Public Health* **2022**, *19*, 14927. [[CrossRef](#)]
73. Chen, Y. An extended patch-based cellular automaton to simulate horizontal and vertical urban growth under the shared socioeconomic pathways. *Comput. Environ. Urban Syst.* **2022**, *91*, 101727. [[CrossRef](#)]
74. Xiong, Y.; Jiao, G.; Zheng, J.; Gao, J.; Xue, Y.; Tian, B.; Cheng, J. Fertility Intention and Influencing Factors for Having a Second Child among Floating Women of Childbearing Age. *Int. J. Environ. Res. Public Health* **2022**, *19*, 16531. [[CrossRef](#)] [[PubMed](#)]
75. QWCB—Quanzhou Water Conservancy Bureau. Quanzhou Water Resources Bulletin in 2020. 2020. Available online: http://slj.quanzhou.gov.cn/zwgk/tzgg/202111/t20211119_2655072.htm (accessed on 6 April 2023).
76. Chen, Y.; Li, X.; Liu, X.; Zhang, Y.; Huang, M. Quantifying the teleconnections between local consumption and domestic land uses in China. *Landsc. Urban Plan.* **2019**, *187*, 60–69. [[CrossRef](#)]
77. Oppenheimer, M.; Glavovic, B.; Hinkel, J.; van de Wal, R.; Magnan, A.K.; Abd-Elgawad, A.; Cai, R.; Cifuentes-Jara, M.; Deconto, R.M.; Ghosh, T. Sea level rise and implications for low lying islands, coasts and communities. In IPCC Special Report on the Ocean and Cryosphere in a Changing Climate. 2019. Available online: <https://www.ipcc.ch/srocc/chapter/chapter-4-sea-level-rise-and-implications-for-low-lying-islands-coasts-and-communities/> (accessed on 15 April 2023).

Disclaimer/Publisher's Note: The statements, opinions and data contained in all publications are solely those of the individual author(s) and contributor(s) and not of MDPI and/or the editor(s). MDPI and/or the editor(s) disclaim responsibility for any injury to people or property resulting from any ideas, methods, instructions or products referred to in the content.